International Journal of Automotive Technology, Vol. 20, No. 2, pp. 411–421 (2019)
DOI 10.1007/s12239–019–0040–9

pISSN 1229–9138/ eISSN 1976–3832

EXPERIMENTAL STUDY OF PARTICULATE EMISSION CHARACTERISTICS FROM A GASOLINE DIRECT INJECTION ENGINE DURING STARTING PROCESS

Yan Su[1, 2], Fangxi Xie[1, 2)*], Wei Hong[1, 2)], Xiaoping Li[1, 2)] and Tingting Hu[3)]

[1)]State Key Laboratory of Automobile Dynamic Simulation and Control, Jilin University, Changchun 130025, China
[2)]College of Automotive Engineering, Jilin University, Changchun 130025, China
[3)]Inspection and Quarantine Technology Center, Jilin Entry Exit Inspect & Quarantine Bur, 1301 Puyang Street, Changchun 130062, China

(Received 23 July 2018; Revised 22 September 2018; Accepted 20 October 2018)

ABSTRACT–The engine starting process presents high particulate emissions in exhaust. This study gives a systematic investigation on particulate emission characteristics, including particulate matter (PM) mass, soluble organic fraction (SOF) mass, C10-C26 n-Alkanes and particle-bound polycyclic aromatic hydrocarbons (PAHs), that have been emitted from a gasoline direct injection (GDI) engine measured by Gas chromatography–mass spectrometry during starting period. The results show that particulate emissions under the warm coolant start condition decline dramatically compared with the cold start condition. 90 % of particulate number (PN) emitted during the cold and warm start periods generally are nucleation-mode particles. Over 50 % PM mass and PAHs emissions are emitted in the first 0–13 s stage. SOF mass accounts more than 60 % in PM mass emissions, especially under the warm coolant start condition. Some C23-C26 n-Alkanes are detected under the cold start condition which demonstrates that partial particulate composition directly comes from lubricant. The concentration of the two ring PAHs is the lowest among PAHs while the four to six ring PAHs are higher under the cold start operation. The toxicity of PAHs which is evaluated by Benzo(a)pyrene equivalent toxicity (BEQ) value of the total PAHs emissions shows a decline of 66.83 % under the warm start condition.

KEY WORDS : Polycyclic aromatic hydrocarbons, Particulate matter emission, Gasoline direct injection engine, Start condition

1. INTRODUCTION

Gasoline direct injection (GDI) engines have better transient response and fuel economy than port fuel injection (PFI) engines. The combination of turbo-charging and downsizing technology on a GDI engine achieves a high fuel efficient (Bandel *et al*., 2006; Petitjean *et al*., 2004). The share of GDI engines has grown rapidly and it is expected that there will be more vehicles produced with GDI engines than PFI engines by 2020 (Zimmerman *et al*., 2016). However, GDI engines usually emit more particulate matter (PM), smaller particle size in particular, than port fuel injection (PFI) engines (Chan *et al*., 2013; Sobotowski *et al*., 2015; Zhang and McMahon, 2012), which is easily transported through the upper respiratory tract into the bronchioles and alveoli of the lungs and brings greater threat to human health (Dockery and Pope, 1994; Gauderman *et al*., 2015; Mariraj Mohan, 2016; Tang *et al*., 2012). The vehicles with GDI engines are subject to the PM standard, a limit of 4.5 mg/km for Euro 6 (The European Parliament and the Council of the European Union, 2009). The EU has proposed a solid particle PN (#/km) limit which is from 6.0×10^{11}-6.0×10^{12} (#/km) in 2014 to 6.0×10^{11} (#/km) in 2017 in Euro 6b and Euro 6c for the type-approval GDI light-duty vehicles (LDVs) (Myung *et al*., 2014). The particulates emitted by internal combustion engines have many properties, such as particle size, number, surface area and chemical composition. They not only affect particulate toxicity, visibility and nucleation, but also have influence on secondary organic aerosols (Egebäck *et al*., 2005; Ghadikolaei, 2016).

The origin of particulate emissions from engine is complex. It is related to the engine fuel, engine type and engine working condition. Some studies were conducted on GDI and PFI engines based on driving cycles like Federal Test Procedure (FTP) and New European Driving Cycle (NEDC) (Khalek *et al*., 2010). The study (Maricq *et al*., 1999) about particulate emissions from a direct-injection spark ignition (DISI) engine under FTP drive cycle showed PM emissions increased when the operation changed from homogeneous charge to stratified charge. Some researchers investigated the relationship between particulate matter and engine operation condition from a GDI engine during cold start. They found that the number

**Corresponding author.* e-mail: xiefx2011@jlu.edu.cn

of fine particles (5 ~ 23 nm) decreased while coolant's temperature rose (Whelan *et al*., 2012). The particle mass and number emission from GDI vehicle decreased as coolant's temperature rose after cold start (Aakko and Nylund, 2003). Studies have shown that PM and PN emissions from vehicles with GDI engines over NEDC or FTP are more than PFI engines and less than non-DPF diesel engines (Aakko and Nylund, 2003; Braisher *et al*., 2010; Kokko *et al*., 2000). After Euro III, the driving cycles took the first 40 seconds of idle operation into the start-up phase because 60 % to 80 % of unburned HC emissions occur within this period (Carter *et al*., 1998). As vehicle with GDI engine emits approximately 50 % of PN within 200 seconds of cold start operation (Peckham *et al*., 2011), and nano-particle concentration during cold start presents two to three orders of magnitude higher than steady state operation (Whelan *et al*., 2010), a deeper research on PM emissions emitted from the first 40 seconds of cold starting process seems to be necessary. Thus, it is important to study on characteristics of PM emissions from GDI engines under start conditions.

With growing number of motor vehicles, their exhaust emissions have become a major source of polycyclic aromatic hydrocarbons (PAHs) (Riddle *et al*., 2007; Tsai *et al*., 2004). According to U.S. Environmental Protection Agency (EPA) standard, 16 PAHs are the priority pollutants to be monitored due to their toxicity on human health (Aakko and Nylund, 2003). PAHs are also considered as soot particle precursors (An *et al*., 2016; Eastwood, 2008). However, few researches have been performed on evaluation of the amount particulate-bound PAHs generated from a GDI engine, especially under start conditions. In order to explore soot particle formation mechanism, it is necessary to pose experimental study on particulate-bound PAHs in the exhaust emissions of GDI engines.

This study investigates the particulate emission characteristics of the GDI engine during the starting process and the chemical composition is also under discussion. PM concentration was measured by an Engine Exhaust Particle Sizer (EEPS Model 3090 TSI Inc.). PAHs and soot particles were sampled under start conditions with a bag sampling system. The PAHs were analyzed qualitatively and quantitatively by a gas chromatography–mass spectrometry (GC–MS).

2. EXPERIMENTAL APPARATUS AND PROCEDURE

2.1. Engine and Experimental System

The engine used in this investigation was an in-line four cylinders, turbo-charged VW1.4L GDI engine. Its specifications are shown in Table 1.

Test fuel was commercial gasoline and the octane number was 97 according Research Octane Number (RON). Its specifications are shown in Table 2. For all tests, the fuel was kept at the same temperature at 20 °C as ambient condition, which was the engine common start condition.

Table 1. GDI engine specifications.

Engine parameters	Specifications
Bore × Stroke	75.6 mm × 76.5 mm
Displacement	1.4 L
Compression ratio	10 : 1
Injector	Multi-hole nozzle
Combustion system	Charge motion-guided GDI
Rated power	96 kW / 5000 rpm
Peak torque	220 N·m / 1750 rpm

Table 2. Gasoline properties.

Gasoline properties	Specifications
Aromatic content (Volume fraction)/%	39.6
Olefinic content (Volume fraction)/%	11.0
Vapor pressure/kPa	56.50
Octane number	97.9
Density (20 °C)/(kg/m^3)	760
Oxygen content (Mass percentage)/%	1.78
Carbon hydrogen ratio	82.65 / 12.51

The operating parameters such as ignition and injection timings were controlled with an electric control unit (ECU), which was supported by the engine manufacture. The parameters couldn't be modified online during the test. There was no split injection during start. In order to monitor the mixture control strategy, an additional lambda sensor, BOSCH LSU 4.9, was mounted upstream from the three way catalytic converter. An ETAS lambda meter ES630 was used to measure the excess air coefficient λ. The λ test range was from 0.700 to 32.767. ES630 had an analog voltage output port. Output gain was λ/V and output frequency was 20 Hz. A RBH8362 data acquisition card was adopted to collect the voltage signal. The acquisition frequency was 1 kHz. So that the changes of excess air coefficient could be obtained under all start conditions. The engine speed was measured by an eddy dynamometer which was produced by Nanfeng. The measurement point was upstream of the catalytic converter. Other testing devices were shown in Figure 1.

2.2. PM Concentration Measurement

The sampling probe was placed into exhaust pipe and PM concentration was measured with EEPS 3090 (Ayala and Herner, 2005; Quiros *et al*., 2015). EEPS 3090 detected PN in 32 channels between 5.6 and 560 nm. It collected data at

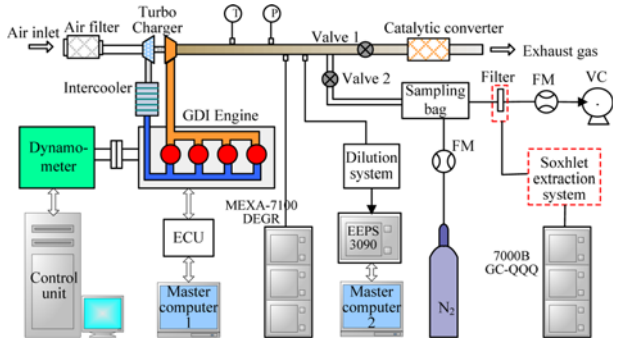

Figure 1. Experimental system sketch.

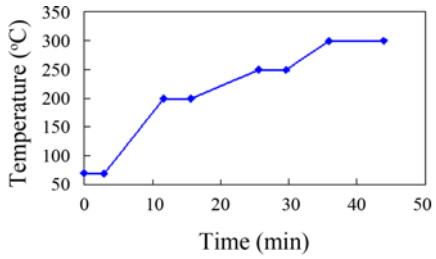

Figure 2. Heat-up curve of GC-MS.

10 Hz. A two-stage dilution system was used to dilute the exhaust before it entered EEPS. The exhaust was heated and diluted by the first stage dilution system, which consists of a heating pipe and an evaporation tube whose temperature were kept at 200 °C and 300 °C, respectively. The first stage dilution ratio was controlled about 10. The second stage dilution system was a cold dilution to drop the exhaust temperature and dilute it further. The primary and secondary dilution ratios could be regulated respectively. The total dilution ratio was kept about 100.

MEXA-7100DEGR of HORIBA was used to measure real-time hydrocarbon (HC) emission changing history during start.

2.3. PM Chemical Composition Measurements

Exhaust gas was collected by a bag which was pre-filled with N_2 for cooling exhaust. The process was controlled by an electrical valve. The sampling time lasted 13 s or 40 s during engine start. Before collecting exhaust gas, empty comparison tests without exhaust were conducted to minimize thermophoretic influence of bags. The flows of N_2 and diluted exhaust were measured by two flow meters respectively and the dilution ratio was calculated. The diluted exhaust was vacuumed from the sampling bag by a pump and particulate emissions were sampled by a woven glass standard filter, which was 47 mm under Federal Test Procedure (FTP). Particulate mass was measured with an electronic analytical balance AE163 made by Mettler.

Soluble organic fraction (SOF) was extracted from the filter with methylene chloride by a Soxhlet extraction system. Then it was condensed to 1ml. C10-C26 n-Alkanes emissions in extracted SOF were measured with GC2014C made by Shimadzu. RTX-1 column was used to detect C10-C26 n-Alkanes. GC2014C was calibrated by a standard sample which contains 17 n-Alkanes from C10-C26. It outputted a proportional electrical signal based on the component concentration of samples and provided qualitative and quantitative analysis.

GC-MS (7000B GC-QQQ, Agilent) was used to analyze PAHs qualitatively and quantitatively. The operational

Table 3. GC-MS operational parameters.

Name	Specification
GC temperature	280 °C
Carrier gas	High purity helium
Flow rate	1.0 L/min
Injection mode	Splitless injection
Scan mode	Selected Reaction Monitoring (SRM)
DB-5MS	30 m × 0.25 mm × 0.25 μm

Table 4. Characteristic parameters of 16 PAHs.

Species name	Abbre-viation	Molecular formula	Structural formula	Number of rings
Naphthalene	Nap	$C_{10}H_8$		2
Acenaphthene	Acp	$C_{12}H_{10}$		3
Acenaphthylene	Acpy	$C_{12}H_8$		3
Fluorene	Flu	$C_{13}H_{10}$		3
Phenanthrene	PA	$C_{14}H_{10}$		3
Anthracene	Ant	$C_{14}H_{10}$		3
Fluoranthene	FL	$C_{16}H_{10}$		4
Pyrene	Pyr	$C_{16}H_{10}$		4
Benzo[a]Anthracene	BaA	$C_{18}H_{12}$		4
Chrysene	CHR	$C_{18}H_{12}$	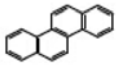	4
Benzo[b]Fluoranthene	BbF	$C_{20}H_{12}$	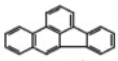	5
Benzo[k]Fluoranthene	BkF	$C_{20}H_{12}$	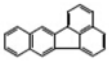	5
Benzo[a]Pyrene	BaP	$C_{20}H_{12}$	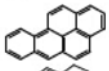	5
Indeno[1,2,3-cd]Pyrene	IND	$C_{22}H_{12}$	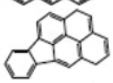	6
Dibenz[a,h]Anthracene	DBAh	$C_{22}H_{12}$	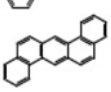	6
Benzo[g,h,i]Perylene	BghiP	$C_{22}H_{14}$		6

Table 5. Calibration curve and the retention time for 16 PAHs.

Species name	Retention time (min)	R^2	Calibration curve
Naphthalene	7.640	0.9999	y = 819929.928472x + 616.614239
Acenaphthene	10.317	0.9999	y = 1178811.251176x – 866.691404
Acenaphthylene	10.626	0.9995	y = 346270.142804x – 1731.216924
Fluorene	11.445	0.9998	y = 1741956.644141x – 3391.951993
Phenanthrene	13.253	0.9998	y = 947634.843027x – 2428.077734
Anthracene	13.361	0.9998	y = 1310351.233401x – 3075.554735
Fluoranthene	17.406	0.9994	y = 542027.943768x – 3389.876077
Pyrene	18.332	0.9993	y = 606576.688954x – 3606.497862
Benzo[a]Anthracene	24.013	0.9992	y = 2153185.494850x – 30512.495529
Chrysene	24.186	0.9993	y = 1261934.061748x – 7828.987838
Benzo[b]Fluoranthene	29.578	0.9998	y = 1540925.018169x – 33177.757036
Benzo[k]Fluoranthene	29.741	0.9983	y = 1603259.079177x – 21060.830360
Benzo[a]Pyrene	31.326	0.9983	y = 1603259.079177x – 216060.830360
Indeno[1,2,3-cd]Pyrene	35.727	0.9981	y = 147464.040647x – 2540.436808
Dibenz[a,h]Anthracene	35.893	0.9997	y = 257868.592819x – 7479.463818
Benzo[g,h,i]Perylene	36.449	0.9983	y = 800634.260362x – 18108.081096

parameters are shown in Table 3. Temperature programming was that GC temperature began from 70 °C (held for 3 minutes), then increased at the speed of 15 °C/min to 200 °C (held for 4 minutes), then continued at the speed of 5 °C/min to 250 °C (held for 4 minutes), and finally ramped up at the speed of 8 °C/min to 300 °C (held for 8 minutes). The heat-up curve is shown as Figure 2.

In order to carry out quantitative analysis of PAHs, GC–MS was calibrated with a standard solution containing 16 EPA-PAH compounds in acetonitrile solvent. 7 concentrations were selected for the standard solution: 10 ng/mL, 20 ng/mL, 50 ng/mL, 100 ng/mL, 200 ng/mL, 500 ng/mL, 1000 ng/mL. The characteristic parameters (Lee *et al*., 2004; Lei *et al*., 2004) and the retention time for each species of standard 16 PAHs compounds are shown in Table 4. Linear regression was carried out according to the calibration results. The calibration curve for each species of 16 PAHs is also shown in Table 5. The coefficient of determination R^2 for each specie calibration curve could reach 99.81 % or more.

Table 6. Testing matrix.

Coolant temperature	0 ~ 40 s	0 ~ 13 s
HC concentration	20/40/60/80 °C	×
PN concentration of distribution	20/40/60/80 °C	×
PM mass	20/40/60/80 °C	20/40/60/80 °C
SOF mass	20/40/60/80 °C	20/40/60/80 °C
N-Alkanes	20/80 °C	20/80 °C
16 PAHs	20/80 °C	20/80 °C

2.4. Experimental Procedure

Effects of coolant's temperature on PM emissions and chemical compositions were examined over the first 40s after engine started.

Testing procedure and matrix are given in Tables 6 and 7. Under warm start conditions, coolant was heated up to the required temperature by a heating system before engine

Table 7. Testing procedure.

Step	Procedure	Testing object	Device
1	Exhaust collecting/PM distribution measuring/speed measuring	PM/HC concentration	Engine bench/bag/EEPS3090/MEXA-7100DEGR
2	Filtering	Sampled exhaust	Teflon filter/vacuum fan
3	Weighting	Filtered residue	Weight balance
4	Soxhlet extracting	Filtered residue	Soxhlet extraction system
5	Chemical analyzing	extraction	GC-MC

started. The coolant was heated with a heater and circulated by a pump between the external cooling system and the engine's internal coolant system. When the temperature reached the set temperature, the heating was stopped and the engine was started. This method was more effective than running the engine to a fixed warm start condition. All experiments were carried out at ambient temperature of 20 °C. The test was conducted 3 times and the results had fair stability and repeatability.

3. RESULTS AND DISCUSSION

3.1. PM Emissions during Starting Process

The start operation of an engine is transient. During starting process, the engine speed varies from 0 r/min to over idle speed and then decreases gradually to a stabilized idle speed. According to the speed diversification, air charging, fuel injection and cylinder wall temperature vary simultaneously. Figure 3 shows the engine speed changing histories under different coolant's temperatures. The higher the coolant temperature is, the sooner the stable idle state can be reached. No matter under what conditions, the engine starting process only needs less than 5 seconds for ramping up to maximum speed, then slowly declines to idle speed. In order to gain a full understanding on PM

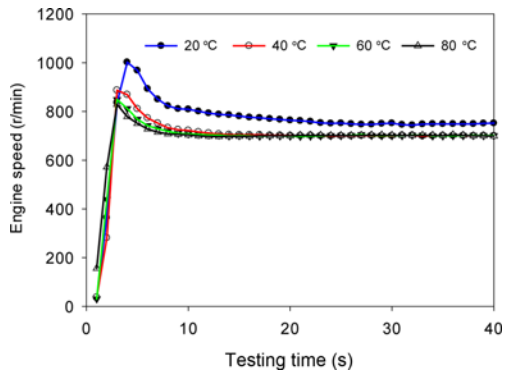

Figure 3. Effect of coolant's temperature on engine speed during start.

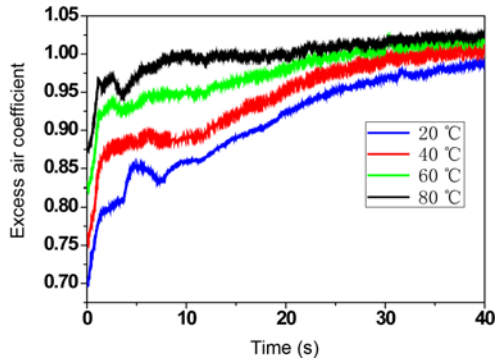

Figure 4. Excess air coefficient changing histories under different coolant's temperatures.

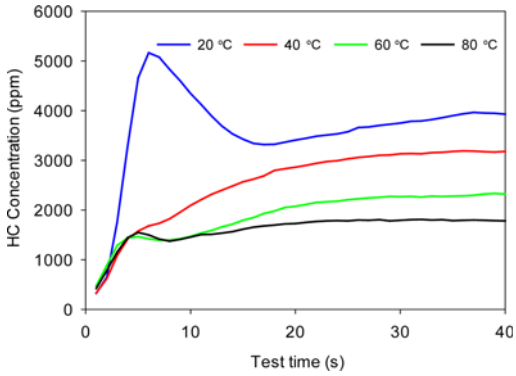

Figure 5. Effect of different coolant's temperatures on HC concentration.

emissions during starting process, testing time (0 ~ 40 s) is divided into two stages: 0 ~ 13 s (on the way to idle speed) and 14 ~ 40 s (idle speed).

The excess air coefficient changing histories during starting process according different coolant's temperatures are shown in Figure 4. While the engine starts under lower coolant's temperature condition, the combustion chamber wall is cold. The lubricating oil becomes thicker and the friction resistance between the engine moving components increases. The crank speed decreases and the gas leakage from pistons increases. The lower wall temperature also makes mixture formation poor. So more rich mixture is required to start engine successfully under such deteriorated conditions. Along with the coolant's temperature rising, the starting process becomes more and more readily and needs less mixture. The excess air coefficient of the mixture also becomes leaner. As soon as the engine reaches peak speed, ECU controls the excess air coefficient increasing to stoichiometric ratio gradually.

Figure 5 shows changes of HC concentrations during starting process. Compared Figure 5 and Figure 3, Figure 4, the result of Figure 5 shows time delay in measurement, because the sampling line of the analyzer is long.

Figure 6 shows PN changing histories under different coolant's temperatures. These two figures show that PN and HC concentrations changing histories present a

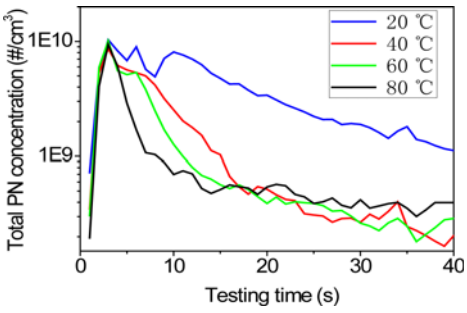

Figure 6. Effect of different coolant's temperatures on PN concentration changing history.

significant difference as coolant's temperature increases. From Figure 6, when the engine starts at coolant's temperature of 20 °C, the peak PN concentration is 1.0×10^{10} which appears in the first 3 seconds, then decreases as time elapses. According to Figure 4, more rich mixture regions lead to production of PM. The lower coolant's temperature is, the more incomplete evaporation occurs. The same consequence can be seen in Figure 5 that the peak HC concentration arrives at 5166 ppm which also occurs in the first 3 seconds. At the beginning of warm coolant start conditions, the peak PN concentrations for three different temperatures arrive at a very similar level of the cold start condition, i.e. between 8.69×10^{9} and 1.01×10^{10}. However, after approximate 8 seconds, the concentrations dramatically decline compared with the cold start condition.

When engine starts under the cold start condition, more fuel is injected into the combustion chamber to ensure engine start successfully, however, the vaporization of gasoline fuel deteriorates because combustion chamber wall is at low temperature, which causes plenty of unburned hydrocarbons condensed in the exhaust pipe. For warm start conditions, the mixture formation improves gradually due to the coolant's temperature rising; thus the HC emissions decrease.

Each channel PN data measured by EEPS 3090 is shown in Figure 7. PM can be classified into two modes by particulate diameter: nucleation-mode (< 50 nm diameter) and accumulation-mode (~ 50 to 500 nm), as described in Kittelson (1998). The total PN concentrations during 40s starting process of different particle diameter channels are calculated in Figure 8. It can be seen that over 90 % particles during the cold start and warm coolant start conditions are nucleation-mode particles. While the coolant's temperature is changed from 20 °C to 40 °C, the concentrations of PM, nucleation-mode particles and accumulation-mode particles are reduced by a factor of 2.48, 2.39 and 3.77 respectively, which suggests that accumulation-mode particles dominate in the decline of total PM concentration. When the coolant's temperature is changed from 40 to 80 °C, the concentrations of nucleation-mode and accumulation-mode particles decrease slightly and gradually in the same trend of PM concentration. Some researches related to nanoparticle composition show that nucleation mode particles of engine exhaust mainly from volatile precursors and this conclusion fits for both gasoline and diesel engines (Ntziachristos *et al*., 2004). During cold starting process more nucleation mode particles followed with more HC emissions indicates that there are some similarities for GDI engines. This can also be proved by following experiment on C10-C16 n-Alkanes and PAHs emissions.

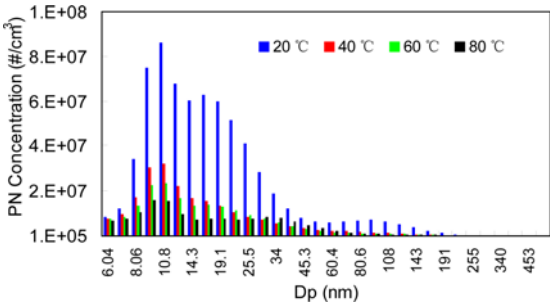

Figure 7. Effect of different coolant's temperatures on the particulate size distribution.

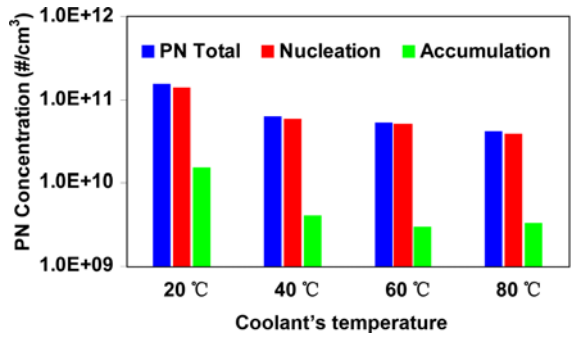

Figure 8. Effect of different coolant's temperatures on the concentrations of accumulation-mode and nucleation-mode particles.

3.2. PM Mass Emissions at Different Stage

Comparison of PM and SOF mass emissions emitted from the engine during 0 ~ 13 s and 0 ~ 40 s are shown in Figure 9. As 0 ~ 40 s, PM mass declines roughly by a factor of 3.6 while the coolant's temperature is changed from 20 to 40 °C, and keeps steady from 40 to 80 °C, the main reason is that once coolant reached 40 °C, mixture formation improves due to engine body temperature rises rapidly. As 0 ~ 13 s, PM mass shows the same reduction trend to 0 ~ 40 s.

The proportion of 0 ~ 13 s PM mass in 0 ~ 40 s and 0 ~ 13 s SOF mass in 0 ~ 40 s are calculated as shown in Figure 10. It can be seen that PM mass within 0 ~ 13 s accounts for 57 % under cold start condition. While coolant's temperature rises, it accounts for more proportion. It can be

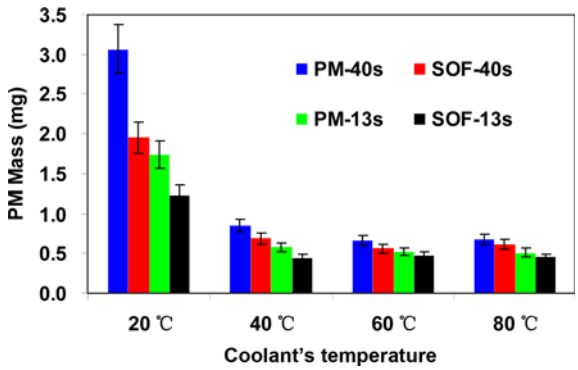

Figure 9. Comparison of PM and SOF mass emitted from GDI engine during 0 ~ 13 s and 0 ~ 40 s.

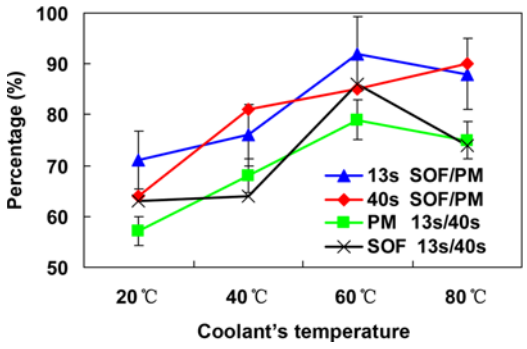

Figure 10. Comparison of SOF mass proportion in PM mass emitted during 0 ~ 13 s and 0 ~ 40 s.

concluded that the most of PM mass is generated during this stage. Without consideration of chemical properties, once coolant reaches 40 °C, the total PM mass will stay stable. While under higher coolant's temperature condition, there is no distinct improvement. The proportion of 0 ~ 13 s SOF mass in 0 ~ 40 s shows similar history to PM mass emission.

The proportions of SOF mass in PM mass during 0 ~ 13 s and 0 ~ 40 s are also calculated respectively as shown in Figure 10. SOF mass accounts more than 60 % in PM mass emission, especially under the warm coolant condition. With increasing of the coolant's temperature, SOF decreases in quantity, but the proportion in PM increases. Under the cold start condition, more fuel injected into cylinder leads more inhomogeneous mixture and wall wetting. All of these enhance soot formation.

3.3. N-Alkanes Emissions

C10-C26 n-Alkanes emissions presented in this section were measured by GC2014C. The typical composition of gasoline is as follows: 6 ~ 13 % alkanes and alkenes; 25 ~ 40 % isoalkanes; 4 ~ 11 % cycloalkanes and cycloalkenes; 25 ~ 50 % aromatics (IARC, 1989). The carbon number is from C5 to C13. C10-C26 n-Alkanes in gasoline are analyzed by GC2014C as shown in Figure 11.

The effect of coolant's temperature on n-Alkanes in PM emissions can be analyzed from Figure 12. The

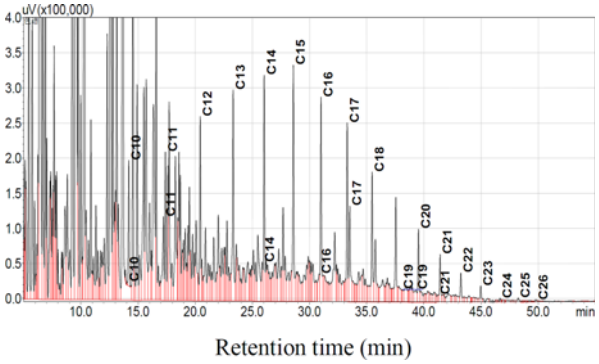

Figure 11. C10-C26 n-Alkanes in gasoline components.

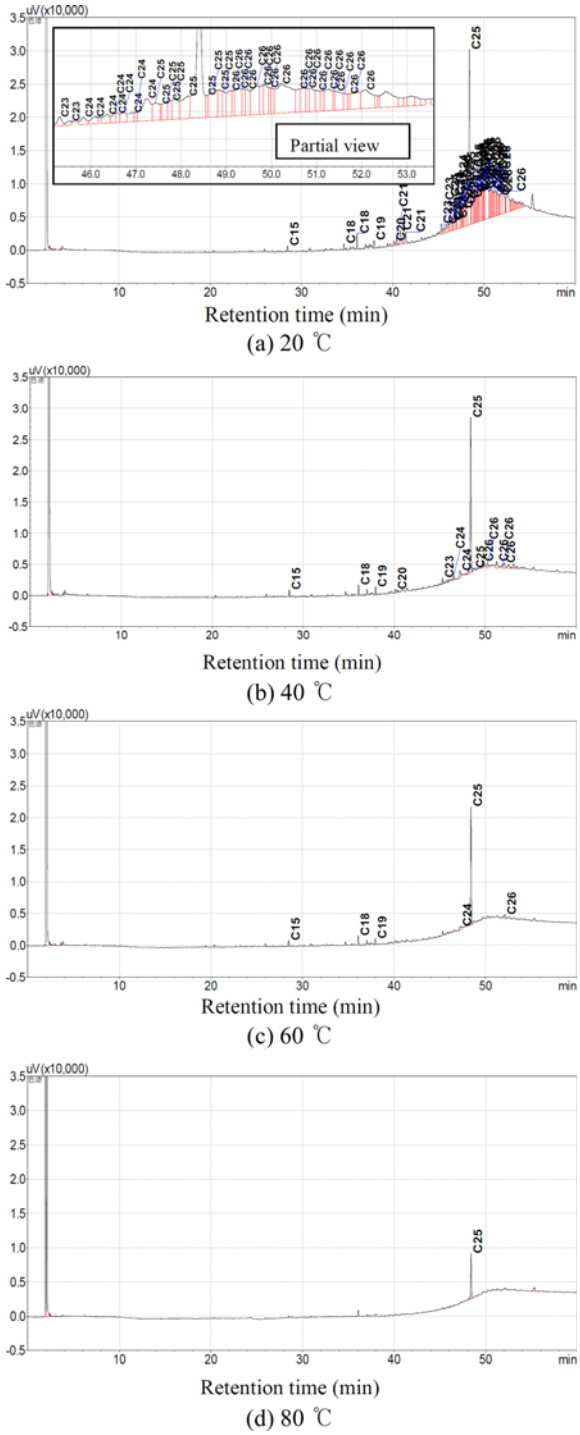

Figure 12. Effect of different coolant's temperatures on n-Alkanes emissions.

concentration and the amount of n-Alkanes both decrease as coolant's temperature increases. There are few C24-C26 n-Alkanes in gasoline (Schauer *et al*., 2002). But from Figure 12, there are more C23-C26 n-Alkanes in PM under the cold start condition than the warm coolant start condition. It can be inferred that some particulate

compositions directly come from lubricating oil and some unburned gasolines under cold starting process (Lechner *et al*., 2002). Though there are no obvious improvement of PM mass from 40 ℃ to 80 ℃, n-Alkanes emissions become much lower with coolant temperature rising despite lubricating oil influence.

3.4. Particle-bound PAHs Emissions

16 PAHs emissions during starting process were measured by Agilent 7000B GC-QQQ. PAHs distribution can be seen from Figure 13. As shown in Figure 13 (a), within 0 ~ 40 s stage, concentrations of naphthalene, acenaphthylene, fluorine, anthracene and dibenz(a,h)anthracene are the lowest. Regardless of naphthalene, acenaphthene, acenaphthylene and fluorine, concentrations of the rest PAHs during 0 ~ 13 s account for 52.5 to 80.0 % of total PAHs within 0 ~ 40 s. Compared Figure 13 (a) with 13 (b), the concentrations of most PAHs have shown a dramatic decline except naphthalene, acenaphthylene, phenanthrene, anthracene and dibenz(a,h)anthracene. This can be explained that PAHs consist of hydrocarbon with two or more benzene rings as defined, and HC emissions under the warm coolant start condition are lower than the cold start condition, which leads to less PAHs emissions. Under the cold start condition, the total concentration of 0 ~ 13 s stage is 8160.37 ppb, which represents 65.05 % of whole

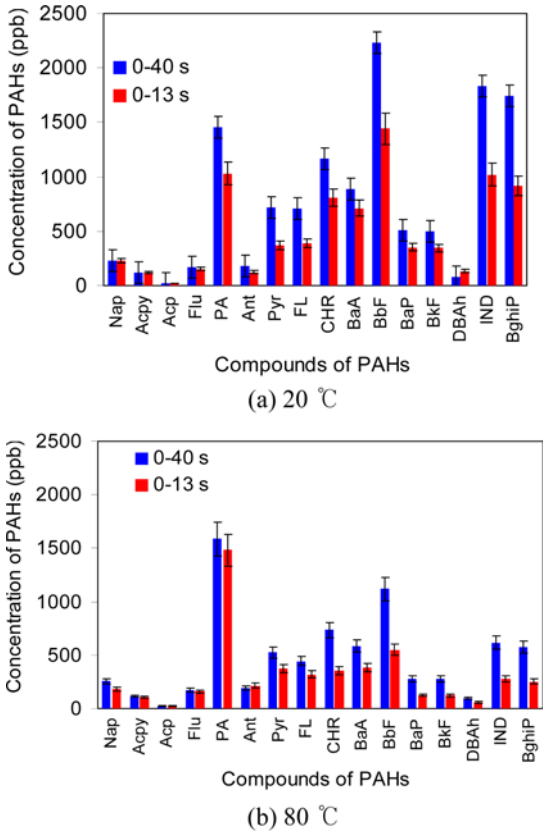

Figure 13. Effect of coolant's temperature on specific PAHs.

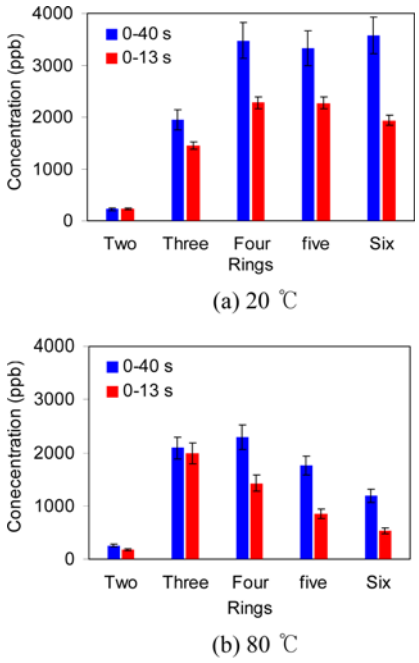

Figure 14. Effect of coolant's temperature on PAHs with different rings.

stage. As for the warm coolant start condition, the percentage of 0 ~ 13 s stage occupied with whole period is 65.55 %. So it can be seen that the first stage is the period not only generating the most of PM mass, but also emitting the most of PAHs emissions.

The toxicity of PAHs compounds is highly dependent on their molecular structure (Maricq *et al*., 1999), so 16 PAHs compounds are divided into five categories according to the number of benzene rings in this section: two rings (naphthalene), three rings (acenaphthylene, acenaphthene, fluorine, phenanthrene, anthracene), four rings (fluoranthene,pyrene, chrysene, benzo(a)anthracene), five rings (benzo(b)fluoranthene, benzo(a)pyrene, benzo(k)fluoranthene, dibenz(a,h)anthracene) and six rings (indeno(1,2,3-cd)pyrene, benzo(g,h,i)perylene).

From Figures 14 (a) and (b), during the whole stage, emissions of two-rings PAHs are the lowest, 225.69 ppb and 256.37 ppb respectively, which could be explained that the formation of PAHs with more rings consumes two-ring naphthalene. For example, one way to generate phenanthrene is the reaction of naphthalene radicals and acetylene (Kazakov *et al*., 1995). The emissions of PAHs with three to six rings are higher for both conditions. PAHs with molecular weight larger than 202, i.e. PAHs with four or more benzene rings, distribute mainly in nano-scale particles (Aceves and Grimalt, 1993), and PM emissions from GDI engine mostly focus on this distribution (Gupta *et al*., 2010). PAHs with four to six rings are higher under the cold start condition than the warm coolant start condition.

Table 8. Toxic equivalency factors of PAHs.

PAHs	TEF	PAHs	TEF
NaP	0.001	Chr	0.01
Acpy	0.001	BaA	0.1
Acp	0.001	BbF	0.1
Flu	0.001	BaP	1
PA	0.001	BkF	0.1
Ant	0.01	DBAh	1
Pyr	0.001	IND	0.1
FL	0.001	BghiP	0.01

3.5. Toxicity Evaluation of PAHs

As benzo(a)pyrene is the strongest carcinogenicity in all PAHs, it has be chosen to evaluate effect of PAHs on human health. Toxic equivalency factors (TEFs) are introduced for evaluation of PAHs. Benzo(a)pyrene equivalent toxicity (BEQ) based on the concept of TEFs is used to characterize the carcinogenicity of PAHs (Nisbet and LaGoy, 1992). BEQ is defined by

$$BEQ = \Sigma Ci \times TEFi \quad (1)$$

where BEQ is total benzo(a)pyrene equivalent toxicity, Ci is the concentration of PAH, and TEFi is toxic equivalency factor of PAH. The toxic equivalency factors of PAHs are listed in Table 8.

Figure 15 is generated by the Equation (1) with the data from Table 8. From Figure 15, under cold start condition, BEQ values of benzo(a)anthracene, benzo(b)fluoranthene, benzo(a)pyrene, benzo(k)fluoranthene, dibenz(a,h) anthracene and indeno(1,2,3-cd)pyrene are the highest among the 16 PAHs emissions, 88.86 ppb, 223.50 ppb, 507.73 ppb, 79.61 ppb and 183.07 ppb respectively, which account for 7.61 %, 19.15 %, 43.50 %, 6.82 % and 15.68 % of the total BEQ values respectively. As for the warm coolant start condition, BEQ values of these five PAHs are 58.34 ppb, 111.85 ppb, 279.40 ppb, 93.71 ppb and 61.75 ppb respectively, which account for 8.97 %, 17.19 %, 42.94 %, 14.40 %, and 9.49 % respectively. BEQ value of the total PAHs emissions under the warm coolant start condition shows a decline of 66.83 % compared with the cold coolant startcondition. In general, higher BEQ value means higher PAHs toxicity. In summary, PAHs toxicity from the GDI engine reduces effectively while engine starts with higher coolant's temperature. It can draw conclusion that the strategy of thermo-management for coolant improvement will benefit PAHs emissions, further step for lower toxicity.

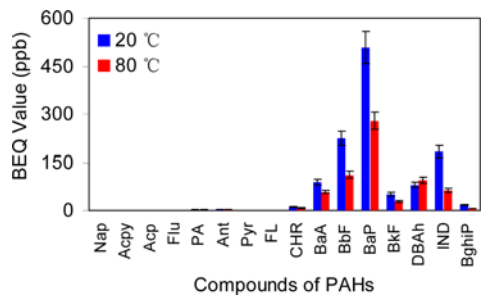

Figure 15. Effect of coolant's temperature on BEQ Values of PAHs.

4. CONCLUSION

A systematic study on particulate emissions under different start conditions was conducted on a GDI engine. The effect of coolant's temperature on PM, SOF, C10-C26 n-Alkanes and particle-bound PAHs emissions were revealed.

The timing of the peak value of the PN concentration of the cold starting process appears similar to that of the warm coolant starting process. Over 90 % of PN emitted during the cold and warm coolant starts is nucleation-mode particles. While the coolant's temperature is changed from 20 °C to 40 °C, the concentrations of PM, nucleation-mode particles and accumulation-mode particles are reduced by a factor of 2.48, 2.39 and 3.77.

PM mass declines roughly by a factor of 3.6 as the coolant's temperature changes from 20 to 40 °C. The first 0 ~ 13 s PM mass accounts for 57 % of the total PM mass in 0 ~ 40 s start period. During the warm coolant start, it increases from 68 to 79 %. SOF accounts more than 60 % in PM mass emissions, especially under warm conditions. Once the coolant temperature exceeds 40 °C, the mass reduction of PM emission is not distinct.

Both the concentration and the quantity of the C10-C26 n-Alkanes decrease with the increasing coolant's temperature. For example, the high carbon number n-Alkanes reduces dramatically as the coolant temperature increases from 40 °C to 80 °C.

The concentration of the two ring PAHs is the lowest among the particle-bound PAHs while the concentrations of the four to six ring PAHs are higher under the cold start operation. The toxicity of PAHs BEQ value of the total PAHs emissions under the warm coolant start condition shows a decline of 66.83 % compared with the cold start condition.

ACKNOWLEDGEMENT–This work was financially supported by the National Natural Science Foundation of China (grant number 51876079 and 51276080) and Jilin Province Science Foundation (grant number 20180201008G X and 20170101131JC).

REFERENCES

Aakko, P. and Nylund, N. O. (2003). Particle emissions at moderate and cold temperatures using different fuels.

SAE Paper No. 2003-01-3285.

Aceves, M. and Grimalt, J. O. (1993). Seasonally dependent size distributions of aliphatic and polycyclic aromatic hydrocarbons in urban aerosols from densely populated areas. *Environmental Science and Technology* **27**, **13**, 2896–2908.

An, Y. Z., Li, X., Teng, S. P., Wang, K., Pei, Y. Q., Qin, J. and Zhao, H. (2016). Development of a soot particle model with PAHs as precursors through simulations and experiments. *Fuel*, **179**, 246–257.

Ayala, A. and Herner, J. D. (2005). Transient ultrafine particle emission measurements with a new fast particle aerosol sizer for a trap equipped diesel truck. *SAE Paper No*. 2005-01-3800.

Bandel, W., Fraidl, G. K., Kapus, P. E., Sikinger, H. and Cowland, C. N. (2006). The turbocharged GDI engine: Boosted synergies for high fuel economy plus ultra-low emission. *SAE Paper No*. 2006-01-1266.

Braisher, M., Stone, R. and Price, P. (2010). Particle number emissions from a range of european vehicles. *SAE Paper No*. 2010-01-0786.

Carter, R. N., Menacherry, P., Pfefferle, W. C., Muench, G. and Roychoudhury, S. (1998). Laboratory evaluation of ultra-short metal monolith catalyst. *SAE Paper No*. 980672.

Chan, T. W., Meloche, E., Kubsh, J., Brezny, R., Rosenblatt, D. and Rideout, G. (2013). Impact of ambient temperature on gaseous and particle emissions from a direct injection gasoline vehicle and its implications on particle filtration. *SAE Int. J. Fuels and Lubricants* **6**, **2**, 350–371.

Dockery, D. W. and Pope, C. A. (1994). Acute respiratory effects of particulate air pollution. *Annual Review of Public Health*, **15**, 107–132.

Eastwood, P. (2008). *Fundamentals: Particulate Emissions from Vehicles.* John Wiley & Sons. Hoboken, New Jersey, USA.

Egebäck, K.-E., Henke, M., Rehnlund, B., Wallin, M. and Westerholm, R. (2005). Blending of Ethanol in Gasoline for Spark Ignition Engines-problem Inventory and Evaporative Measurements. AVL MTC Motortestcenter AB.

Gauderman, W. J., Urman, R., Avol, E., Berhane, K., McConnell, R., Rappaport, E., Chang, R., Lurmann, F. and Gilliland, F. (2015). Association of improved air quality with lung development in children. *New England J. Medicine*, **372**, 905–913.

Ghadikolaei, M. A. (2016). Effect of alcohol blend and fumigation on regulated and unregulated emissions of IC engines – A review. *Renewable and Sustainable Energy Reviews*, **57**, 1440–1495.

Gupta, T., Kothari, A., Srivastava, D. K. and Agarwal, A. K. (2010). Measurement of number and size distribution of particles emitted from a mid-sized transportation multipoint port fuel injection gasoline engine. *Fuel* **89**, **9**, 2230–2233.

IARC (1989). Occupational exposures in petroleum refining; crude oil and major petroleum fuels. *IARC Working Group on the Evaluation of Carcinogenic Risks to Humans*, Lyon, France.

Kazakov, A., Wang, H. and Frenklach, M. (1995). Detailed modeling of soot formation in laminar premixed ethylene flames at a pressure of 10 bar. *Combustion and Flame* **100**, **1-2**, 111–120.

Khalek, I. A., Bougher, T. and Jetter, J. J. (2010). Particle emissions from a 2009 gasoline direct injection engine using different commercially available fuels. *SAE Int. J. Fuels and Lubricants* **3**, **2**, 623–637.

Kittelson, D. B. (1998). Engines and nanoparticles: A review. *J. Aerosol Science* **29**, **5-6**, 575–588.

Kokko, J., Rantanen, L., Pentikäinen, J., Honkanen, T., Aakko, P. and Lappi, M. (2000). Reduced particulate emissions with reformulated gasoline. *SAE Paper No*. 2000-01-2017.

Lechner, G., Knafl, A., Assanis, D. N., Tseregounis, S. I., McMillan, M. L., Tung, S. C., Mulawa, P. A., Bardasz, E. and Cowling, S. (2002). Engine oil effects on the friction and emissions of a light-duty, 2.2 L direct - injection - diesel engine part 1 - engine test results. *SAE Paper No*. 2002-01-2681.

Lee, J. J., Huang, K. L., Yu, Y. C. Y. and Chen, M. S. S. (2004). Laboratory retention of vapor-phase PAHs using XAD adsorbents. *Atmospheric Environment* **38**, **36**, 6185–6193.

Lei, L., Suidan, M. T., Khodadoust, A. P. and Tabak, H. H. (2004). Assessing the bioavailability of PAHs in field-contaminated sediment using XAD-2 assisted desorption. *Environmental Science & Technology* **38**, **6**, 1786–1793.

Maricq, M. M., Podsiadlik, D. H., Brehob, D. D. and Haghgooie, M. (1999). Particulate emissions from a direct-injection spark-ignition (DISI) engine. *SAE Paper No*. 1999-01-1530.

Mariraj Mohan, S. (2016). An overview of particulate dry deposition: Measuring methods, deposition velocity and controlling factors. *Int. J. Environmental Science and Technology* **13**, **1**, 387–402.

Myung, C. L., Ko, A. and Park, S. (2014). Review on characterization of nano-particle emissions and PM morphology from internal combustion engines: Part 1. *Int. J. Automotive Technology* **15**, **2**, 203–218.

Nisbet, I. C. T. and LaGoy, P. K. (1992). Toxic equivalency factors (TEFs) for polycyclic aromatic hydrocarbons (PAHs). *Regulatory Toxicology and Pharmacology* **16**, **3**, 290–300.

Ntziachristos, L., Mamakos, A., Samaras, Z., Mathis, U., Mohr, M., Thompson, N., Stradling, R., Forti, L. and de Serves, C. (2004). Overview of the european "particulates" project on the characterization of exhaust particulate emissions from road vehicles: Results for light-duty vehicles. *SAE Paper No*. 2004-01-1985.

Peckham, M. S., Finch, A., Campbell, B., Price, P. and

Davies, M. T. (2011). Study of particle number emissions from a turbocharged Gasoline Direct Injection (GDI) engine including data from a fast-response particle size spectrometer. *SAE Paper No*. 2011-01-1224.

Petitjean, D., Bernardini, L., Middlemass, C. and Shahed, S. M. (2004). Advanced gasoline engine turbocharging technology for fuel economy improvements. *SAE Paper No*. 2004-01-0988.

Quiros, D. C., Zhang, S., Sardar, S., Kamboures, M. A., Eiges, D., Zhang, M., Jung, H. S., Mccarthy, M. J., Chang, M. C. O., Ayala, A., Zhu, Y. F., Huai, T. and Hu, S. H. (2015). Measuring particulate emissions of light duty passenger vehicles using Integrated Particle Size Distribution (IPSD). *Environmental Science & Technology* **49**, **9**, 5618–5627.

Riddle, S. G., Robert, M. A., Jakober, C. A., Hannigan, M. P. and Kleeman, M. J. (2007). Size distribution of trace organic species emitted from light-duty gasoline vehicles. *Environmental Science & Technology* **41**, **21**, 7464–7471.

Schauer, J. J., Kleeman, M. J., Cass, G. R. and Simoneit, B. R. T. (2002). Measurement of emissions from air pollution sources. 5. C_1-C_{32} organic compounds from gasoline-powered motor vehicles. *Environmental Science & Technology* **36**, **6**, 1169–1180.

Sobotowski, R. A., Butler, A. D. and Guerra, Z. (2015). A pilot study of fuel impacts on PM emissions from light-duty gasoline vehicles. *SAE Int. J. Fuels and Lubricants* **8**, **1**, 214–233.

Tang, M. J., Li, Q. F., Xiao, L. F., Li, Y. P., Jensen, J. L., Liou, T. G. and Zhou, A. H. (2012). Toxicity effects of short term diesel exhaust particles exposure to human Small Airway Epithelial Cells (SAECs) and human lung carcinoma epithelial cells (A549). *Toxicology Letters* **215**, **3**, 181–192.

The European Parliament and the Council of the European Union (2009). Regulation (EC) No. 595/2009 of the European Parliament and of the Council of June 18, 2009 on Type-approval of Motor Vehicles and Engines with Respect to Emissions from Heavy Duty Vehicles (Euro VI) and on Access to Vehicle Repair and Maintenance Information and Amending Regulation (EC) No. 715/2007 and Directive 2007/46/EC and Repealing Directives 80/1269/EEC, 2005/55/EC and 2005/78/EC. *Regulation (EC)*, No 595/2009.

Tsai, P. J., Shih, T. S., Chen, H. L., Lee, W. J., Lai, C. H. and Liou, S. H. (2004). Assessing and predicting the exposures of Polycyclic Aromatic Hydrocarbons (PAHs) and their carcinogenic potencies from vehicle engine exhausts to highway toll station workers. *Atmospheric Environment* **38**, **2**, 333–343.

Whelan, I., Samuel, S., Timoney, D. and Hassaneen, A. (2010). Characteristics of nano-scale particulates from gasoline turbo-intercooled direct-injection engine. *SAE Int. J. Fuels and Lubricants* **3**, **2**, 839–848.

Whelan, I., Smith, W., Timoney, D. and Samuel, S. (2012). The effect of engine operating conditions on engine-out particulate matter from a gasoline direct-injection engine during cold-start. *SAE Paper No*. 2012-01-1711.

Zhang, S. and McMahon, W. (2012). Particulate emissions for LEV II light-duty gasoline direct injection vehicles. *SAE Int. J. Fuels and Lubricants* **5**, **2**, 637–646.

Zimmerman, N., Wang, J. M., Jeong, C. H., Wallace, J. S. and Evans, G. J. (2016). Assessing the climate trade-offs of gasoline direct injection engines. *Environmental Science & Technology* **50**, **15**, 8385–8392.